Title	Rotational band properties of ^{173}W
Author(s)	Wang H. X., Zhang Y. H., Zhou X. H., Liu M. L., Ding B., Li G. S., Hua W., Zhou H. B., Guo S., Qiang Y. H., Oshima Masumi, Koizumi Mitsuo, Toh Yosuke, Kimura Atsushi, Harada Hideo, Furutaka Kazuyoshi, Kitatani Fumito, Nakamura Shoji, Hatsukawa Yuichi, Ota Masayuki, Hara Kaoru, Kin Tadahiro, Meng J.
Citation	Physical Review C, 86(4), p.044305_1-044305_11
Text Version	Publisher's Version
URL	https://jopss.jaea.go.jp/search/servlet/search?5038952
DOI	http://dx.doi.org/10.1103/PhysRevC.86.044305
Right	

Rotational band properties of ^{173}W

H. X. Wang,[1,2] Y. H. Zhang,[1,*] X. H. Zhou,[1] M. L. Liu,[1] B. Ding,[1,2] G. S. Li,[1,2] W. Hua,[1] H. B. Zhou,[1,2] S. Guo,[1] Y. H. Qiang,[1] M. Oshima,[3] M. Koizumi,[3] Y. Toh,[3] A. Kimura,[3] H. Harada,[3] K. Furutaka,[2] F. Kitatani,[2] S. Nakamura,[3] Y. Hatsukawa,[3] M. Ohta,[3] K. Hara,[3] T. Kin,[3] and J. Meng[4,5]

[1]*Institute of Modern Physics, Chinese Academy of Sciences, Lanzhou 730000, China*

[2]*Graduate School of Chinese Academy of Sciences, Beijing 100049, China*

[3]*Japan Atomic Energy Agency, Tokai-Mura, Ibaraki 319-1195, Japan*

[4]*State Key Laboratory of Nuclear Physics and Technology, School of Physics, Peking University, Beijing 100871, China*

[5]*School of Physics and Nuclear Energy Engineering, Beihang University, Beijing 100191, China*

(Received 29 November 2011; revised manuscript received 22 June 2012; published 1 October 2012)

High-spin states in ^{173}W have been studied using the ^{150}Nd(^{28}Si, $5n$)^{173}W reaction at beam energies of 135 and 140 MeV. The previously known bands associated with the $7/2^+[633]$, $5/2^-[512]$, and $1/2^-[521]$ configurations are extended significantly, and the unfavored signature branch of the $1/2^-[521]$ band is established for the first time. The band properties, such as level spacings, band-crossing frequencies, alignment gains, and signature splittings, are discussed with an emphasis on the low-spin signature inversion observed in the $5/2^-[512]$ band. By comparing the experimental $B(M1)/B(E2)$ ratios with the theoretical values, we conclude that the configuration of the $5/2^-[512]$ band is quite pure at low spins without appreciable admixture of the $5/2^-[523]$ orbit, in conflict with the particle rotor model calculated results.

DOI: 10.1103/PhysRevC.86.044305 PACS number(s): 21.10.Re, 23.20.Lv, 25.70.Gh, 27.70.+q

I. INTRODUCTION

For the odd-N prolately deformed nuclei in the $A =$ 160–180 mass region, the neutron Fermi surface is located at the $h_{11/2}$, $i_{13/2}$, $h_{9/2}$, $f_{7/2}$, $f_{5/2}$, and $p_{3/2}$ subshells, and variant types of rotational bands have been observed experimentally [1–7]. The rotational bands exhibit anomalous band-crossing frequencies, interesting aligned angular momenta, large signature splittings, and signature inversions. Among these phenomena, the low-spin signature inversion observed in odd-A nuclei is not well understood [1,6]. Signature quantum number α, describing the invariance of the intrinsic Hamiltonian of an axially deformed nucleus with respect to 180° rotation around a principal axis, is a conserved quantum number [8]. The signature splitting is defined as the difference in energies at a given rotational frequency for a pair of signature partners. For a nuclear system with an odd particle number, the favored and unfavored signatures are defined by $\alpha_f = 1/2 \times (-1)^{j-1/2}$ and $\alpha_{uf} = 1/2 \times (-1)^{j+1/2}$, respectively, where j is the angular momentum of the odd particle. Usually, the favored $\Delta I = 2$ level sequence should be lower in energy than the unfavored sequence. However, this rule is broken in some odd-A nuclei [1,6,9–11]; the expected favored branch lies higher in energy than the unfavored one. This phenomenon is known as signature inversion [9].

Prior to this work, rotational bands associated with the $i_{13/2}$, $5/2^-[512]$, and $1/2^-[521]$ configurations in the ^{171}Hf, ^{173}W, and ^{175}Os isotones were reported [3–5]. Inspecting the existing data, we find that low-spin signature inversions occur in the $5/2^-[512]$ bands in ^{171}Hf [3] and ^{175}Os [5]. In a naive expectation, there should exist a similar low-spin signature inversion in the $5/2^-[512]$ band in ^{173}W. However, the $5/2^-[512]$ band in ^{173}W was not observed to a sufficient high spin to reveal such a phenomenon [4]. The present work aims at extending the level scheme of ^{173}W to higher spin states and trying to identify the signature inversion in the $5/2^-[512]$ band.

II. EXPERIMENT

High-spin levels in ^{173}W were populated via the ^{150}Nd(^{28}Si, $5n\gamma$) reaction. The ^{28}Si beam with an intensity of about 1.0 pnA was provided by the tandem accelerator at the Japan Atomic Energy Agency (JAEA). Beam energies of 135 and 140 MeV were chosen to populate the excited states in ^{173}W on the basis of the excitation function measurements. The target was an oxidized enriched ^{150}Nd foil of 2.0 mg/cm^2 thickness with a 7.8 mg/cm^2 gold backing. The γ-ray detector array GEMINI [12] was used to measure the γ-γ-t coincidence. Here t refers to the relative time difference between any two coincident γ rays detected within ±100 ns. The energy and efficiency calibrations were made using ^{133}Ba and ^{152}Eu standard sources before and after the experiment. Typical energy resolutions were about 2.0–2.5 keV full width at half maximum (FWHM) for the 1332.5-keV line of ^{60}Co.

To determine the multipolarities of the transitions observed experimentally, two asymmetric coincidence matrices were constructed using the γ rays detected at all angles (y axis) against those observed at ∼40° (or 140°) and 90° (x axis), respectively. From these two matrices, the angular distribution asymmetry ratios, defined as $R_{ADO}(\gamma) = I_\gamma(40°)/I_\gamma(90°)$, were extracted from the γ-ray intensities $I_\gamma(40°)$ and $I_\gamma(90°)$ in the coincidence spectra gated by the γ transitions (on the

*yhzhang@impcas.ac.cn

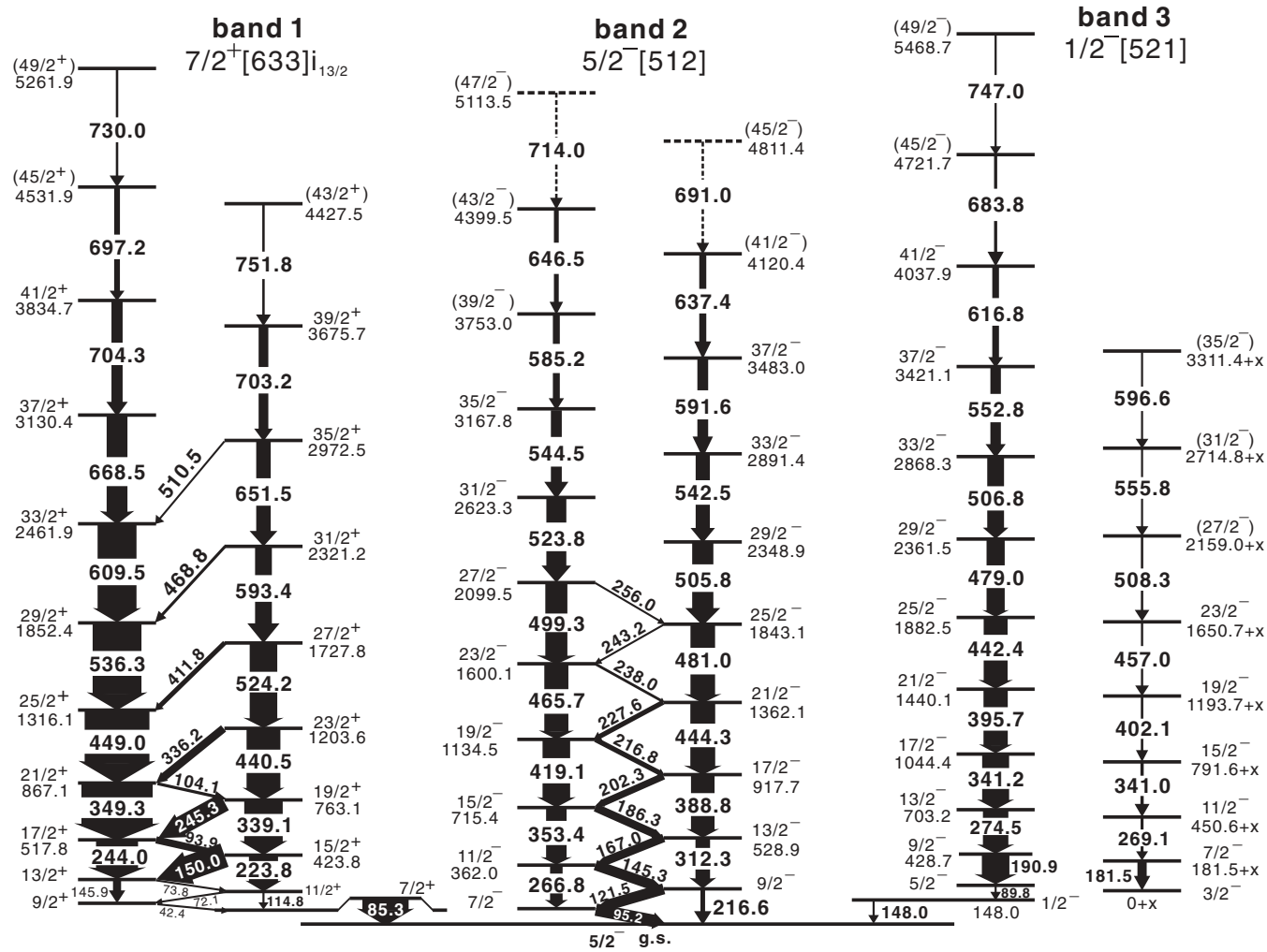

FIG. 1. Level scheme of ^{173}W deduced from this work. The level and transition energies are given in keV and the widths of the arrows indicate the relative γ-transition intensities.

y axis) of any multipolarities. Usually, a single gate was used for strong peaks. For some weak or doublet peaks, the gating transitions were carefully chosen in order to obtain a clear coincidence spectrum in which possible contaminations to the transition of interest can be excluded. In the present geometry, stretched quadrupole transitions ($\Delta I = 2$) were adopted if $R_{ADO}(\gamma)$ values were significantly larger than unity [with an average value of $R_{ADO}(\gamma) = I_\gamma(40^\circ)/I_\gamma(90^\circ) = 1.31 \pm 0.05$ being obtained for the known strong $E2$ transitions in ^{172,174}W], and dipole transitions ($\Delta I = 1$) were assumed if $R_{ADO}(\gamma)$ values were significantly less than 1.0.

III. EXPERIMENTAL RESULTS

Rotational bands in ^{173}W were established in a previous work [4]. This provides an important basis for the present work. Assignments of the observed new γ rays to ^{173}W were based on the coincidences with the known ones. Coincidence spectra were produced for each of the γ rays assigned to ^{173}W. According to coincidence relationships, γ-ray energy sums, and γ-ray relative intensities, a new level scheme for ^{173}W is proposed and shown in Fig. 1. Some brief explanations of the level scheme are given as follows.

Band 1 was most strongly populated. This band was suggested to be associated with the $7/2^+[633]i_{13/2}$ configuration [4]. The present work extends the $\alpha = +1/2$ sequence from $I^\pi = 41/2^+$ to $(49/2^+)$ and the $\alpha = -1/2$ sequence from $I^\pi = 39/2^+$ to $(43/2^+)$. The intra-band transitions at 411.8, 468.8, and 510.5 keV are newly observed. The first two panels of Fig. 2 present the spectra in coincidence with the 651.5- and 536.3-keV transitions, to show the level structure of band 1 and the existence of the new γ rays. Inspecting the spectrum in coincidence with the 536.3-keV transition, one can see that there is clear peak at 440.5 keV, and in fact there is a peak at 536.3 keV in the spectrum in coincidence with the 440.5-keV transition. These indicate that the 440.5-keV transition is in coincidence with the 536.3-keV transition, and there should be a transition from the 1316.1-keV state to the 1203.6-keV state. But this intraband transition of $\approx$112.5 keV was not observed clearly experimentally. This can be explained by considering the theoretical conversion coefficients and the detection

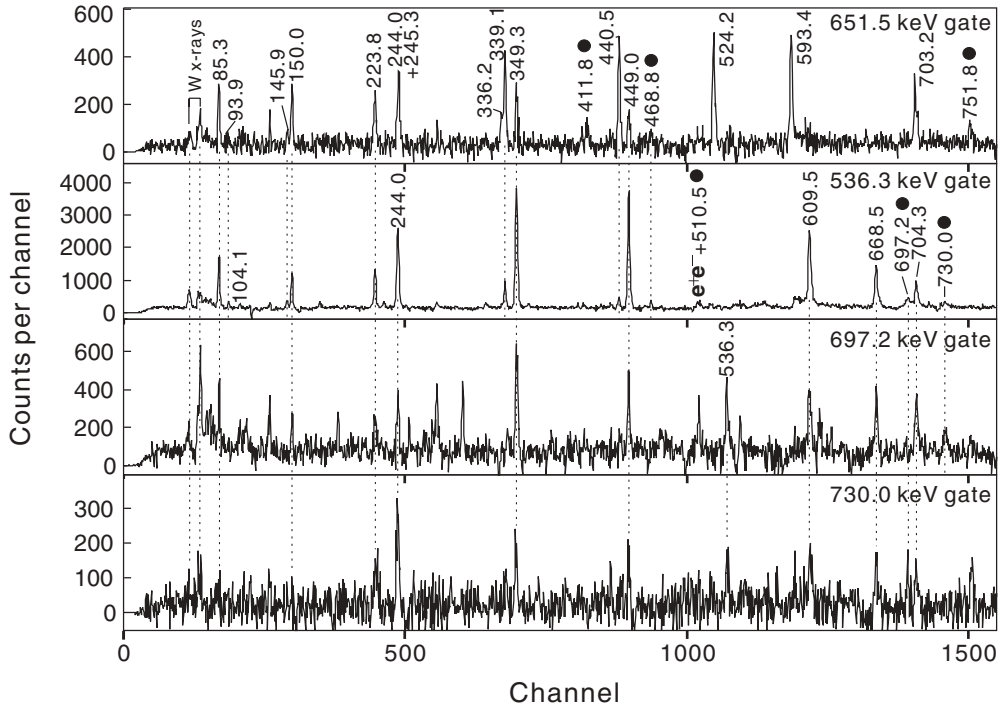

FIG. 2. γ-ray spectra in coincidence with the 651.5-, 536.3-, 697.2-, and 730.0-keV transitions in band 1. The filled circles indicate the new γ rays of ^{173}W observed in the present work. "e^+e^-" means the contamination from e^+e^- annihilation.

efficiencies α_T^{th} for the 440.5- and 112.5-keV transitions. With $\alpha_T^{th}(440.5; E2) = 0.03$, $\alpha_T^{th}(112.5; M1) = 3.50$, and the detection efficiencies for the two transitions 0.86 and 0.92, the relative intensity ratios for ≈112.5- and 440.5-keV γ rays in the spectrum in coincidence with 536.3 keV is about 0.31. The weak peak at 440.5 keV indicates that the peak at ≈112.5 keV is possibly too weak to be observed. We also studied the spectrum in coincidence with the 112.5-keV line, and we found that there are ambiguous peaks at 536.3 and 440.5 keV. Therefore, we did not place this intraband transition in the level scheme. The bottom two panels of Fig. 2 are used especially to show the sequences of the topmost transitions in band 1. It is clear from these two panels that the 697.2- and 730.0-keV transitions form one cascade but not parallel sequences. It is noted that the 73.8-, 72.1-, 42.4-, and 114.8-keV low-energy transitions reported in Ref. [4] were not observed in the present work because of their high conversion natures (see Table I) and low detection efficiencies.

Band 2 was claimed to be built on the $5/2^-[512]$ configuration and known up to the $31/2^-$ and $25/2^-$ states in previous work [4]. We extend the two branches up to $I^\pi = (47/2^-)$ and $I^\pi = (45/2^-)$, respectively. Moreover, the intraband transitions from the 2099.5-keV state to 917.7-keV state are added to band 2. Figure 3 displays the structure of band 2 and the existence of the new transitions. The 511-keV peaks in the spectra may arise from e^+e^- annihilation. This peak exists in the spectra in coincidence with most of the strong transitions in ^{173}W. The bump close to 600 keV in the spectra relates to the background from $^{nat}Ge(n,\gamma)$ reactions. Since the top transitions are decisive for band-crossing frequencies, signature inversion, and the respective theoretical discussion at Sec. IV, Fig. 4 is used in particular to show the placements of the topmost but weak transitions in this band. Ordering of the top transitions, especially the new ones, is based on their relative intensities. In previous work it was suggested that the 544.5-keV transition directly feeds the 2099.5-keV level [4]. Analyzing carefully the coincidence relationships and the relative intensities for the transitions involved, we propose that it is the 523.8-keV transition that populates the 2099.5-keV state, and the 544.5-keV transition should be located above the 523.8-keV transition.

Band 3 was associated with the $1/2^-[521]$ configuration, and only the favored signature branch was observed previously [4]. In the present work, the favored branch is extended by two transitions of 683.8 and 747.0 keV. Most importantly, a weakly populated sequence consisting of the 181.5-, 269.1-, 341.0-, 402.1-, 457.0-, 508.3-, 555.8-, and 596.6-keV transitions is observed and assigned as the unfavored signature branch of band 3. As shown in Fig. 5(a), the 181.5-keV transition shows evident coincidence with all the known transitions of band 3 except the 190.9- and 89.8-keV ones. This indicates that the 181.5-keV transition should be parallel to the 190.9- and 89.8-keV transitions. However, low-energy linking transitions between the two signature partners were not observed experimentally. Consequently, the relative level energies of the two signature branches cannot be determined. The ordering of the transitions in the new sequence of band 3 was determined mainly on the basis of a systematic analysis of the level spacings. In the isotones ^{169}Yb [13], ^{171}Hf [3], and ^{175}Os [5] and the heavier odd-A tungsten isotopes [4,13,14], both of the signature branches of the $1/2^-[521]$ band were observed. The unfavored signature branch of band 3 in ^{173}W fits well into the

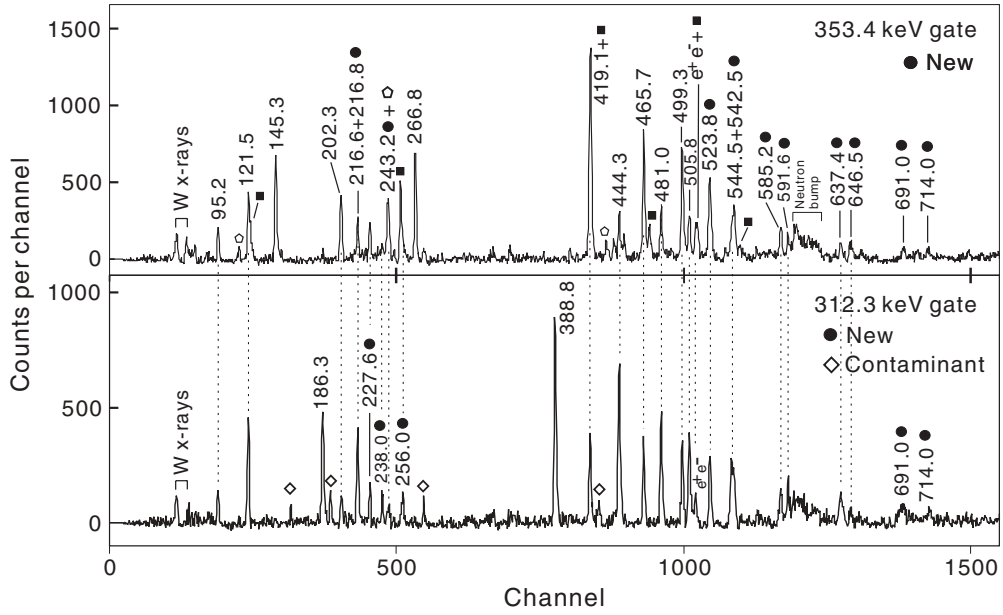

FIG. 3. γ-ray spectra in coincidence with the 353.4- and 312.3-keV transitions in band 2. The filled circles indicate the new γ rays of ^{173}W observed in the present work. The peaks marked by the solid rectangles indicate the γ rays from ^{172}W and the peaks marked by the pentagons indicate the γ rays from ^{174}W. The peak at 511 keV is from the e^+e^- annihilation. The bump close to 600 keV is the background from $^{\text{nat}}$Ge(n,γ) reactions. The $\diamond$ symbols indicate the unknown contaminations.

structure systematics, as discussed in the next section. In the gated spectrum of the favored signature of the $1/2^-[521]$ band of the isotone ^{171}Hf, there is also a 165-keV peak [the transition from $9/2^-\rightarrow 7/2^-$ (see Figs. 1 and 2(f) in Ref. [3])]. In the level scheme of the isotope ^{175}W, there is also a $9/2^-\rightarrow 7/2^-$ transition observed in the $1/2^-[521]$ band (see Figs. 5 and 6 in Ref. [4]). As for why there are no transitions observed from the unfavored signature to the favored one in ^{173}W, we think it is because of their extremely weak intensities that they are not identified undoubtedly; for example, the 89.8-keV transition and the transitions above the $7/2^-$ state in the unfavored branch are so weak that it is hard to confirm their coincidence relationships unambiguously.

In previous work, the ground state of ^{173}W was proposed to be either the $5/2^-[512]$ bandhead or the $1/2^-[521]$ bandhead [4] because the connecting transitions between bands 2 and 3 were not observed, and therefore the level energies in Ref. [4] were given relative to the bandhead of band 2. In the present work, a new 148.0-keV transition linking bands 2 and 3 is observed. Figure 5(d) presents the coincidence spectrum gated by the 148.0-keV transition, together with the ones gated on the 274.5- and 479.0-keV transitions [see Figs. 5(c) and 5(b)] for comparison. It is clear that the 148.0-keV transition is in coincidence with all the known transitions of band 3. The relative intensities of the coincident γ lines indicate that the 148.0-keV transition should be placed at the bottom of band 3. Therefore, we propose that the 148.0-keV transition decays directly from the bandhead of band 3 to the $5/2^-[512]$ state, and the $5/2^-[512]$ state is the ground state. We have to note that the intensity of the 148.0-keV transition is abnormally smaller than that of the 190.9-keV transition, as shown in the coincidence spectrum gated on the 274.5-keV transition [see Fig. 5(c)]. By taking into account the internal conversion for the 148.0-keV transition assuming an $E2$ character, the intensity balance still could not be fulfilled. A possible explanation is that the bandhead of band 3 is an isomer, so that only small decay flux was recorded in the experiment. Using the 148.0- and 190.9-keV transition intensities deduced from the spectrum in coincidence with the 274.5-keV transition and corrected with the internal conversions (see Table I) and detection efficiencies, the lifetime for the $1/2^-[521]$ isomer is estimated to be 1.31(15) μs. In ^{177}Pt [16], the $1/2^-[521]$ isomer was observed with a half-life of 2.2 μs.

For the coupled bands shown in Fig. 1, the branching ratios, which are defined as

$$\lambda = \frac{T_\gamma(I \rightarrow I-2)}{T_\gamma(I \rightarrow I-1)}, \tag{1}$$

were extracted for most transitions. Here $T_\gamma(I \rightarrow I-2)$ and $T_\gamma(I \rightarrow I-1)$ are the γ-ray intensities of the $\Delta I = 2$ and $\Delta I = 1$ transitions, respectively. These intensities were measured in a summed coincidence spectrum gated by the transitions above the state of interest. The branching ratios were used to extract the reduced transition probability ratios, which are defined as [17]

$$\frac{B(M1; I \rightarrow I-1)}{B(E2; I \rightarrow I-2)} = 0.697 \frac{[E_\gamma(I \rightarrow I-2)]^5}{[E_\gamma(I \rightarrow I-1)]^3} \frac{1}{\lambda} \frac{1}{1+\delta^2} \times \left(\frac{\mu_N^2}{e^2\,\mathrm{b}^2}\right), \tag{2}$$

where δ is the $E2/M1$ mixing ratio for the $\Delta I = 1$ transition, and $E_\gamma(I \rightarrow I-1)$ and $E_\gamma(I \rightarrow I-2)$ are the $\Delta I = 1$ and $\Delta I = 2$ transition energies in MeV, respectively. In the present analysis, we assumed $\delta = 0$ (and for $|\delta| < 0.3$, the errors induced are less than 10%).

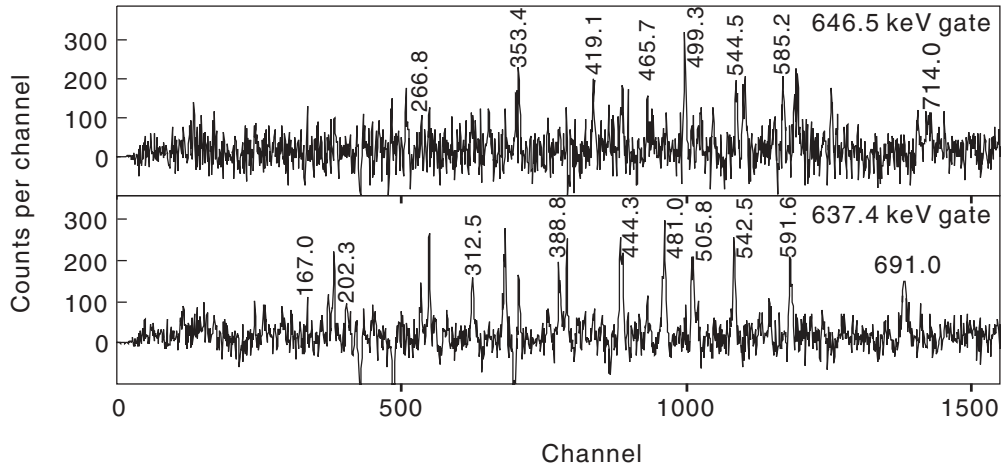

FIG. 4. γ-ray spectra in coincidence with the topmost transitions at 646.5 and 637.4 keV of band 2. The peaks marked correspond to the strong transitions in band 2.

The relative intensities for some uncontaminated γ rays were measured in the total projection spectrum. Most of the relative intensities were extracted from the spectra in coincidence with the bottom transitions in the band. The γ-ray energies, spin-parity assignments, relative intensities, branching ratios, extracted $B(M1)/B(E2)$ values, and the $R_{ADO}(\gamma)$ values are presented in Table II grouped in sequences for each band.

IV. DISCUSSION

In order to study the band properties, it is necessary to transform the experimental excitation energies and spins into the rotating frame [18]. The standard plots of the quasiparticle-aligned angular momenta, i, as a function of rotational frequencies are shown in Fig. 6. The quasiparticle-aligned angular momentum results from the subtraction of a reference angular momentum, $\omega J_0 + \omega^3 J_1$, from the total angular

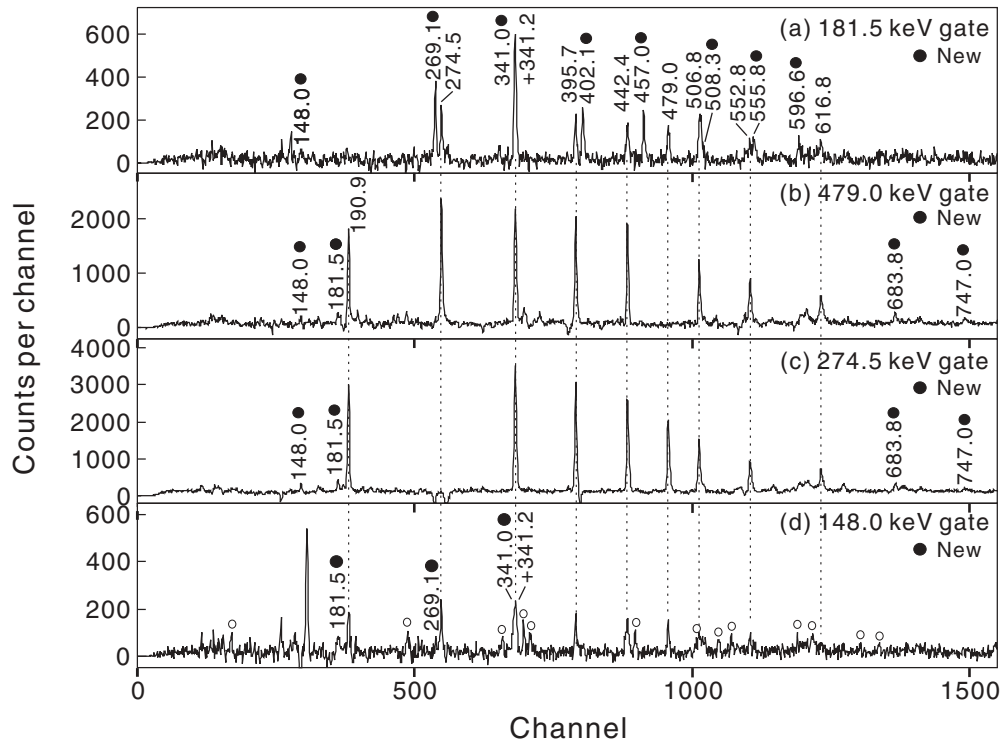

FIG. 5. γ-ray spectra in coincidence with the 181.5-, 479.0-, 274.5-, and 148.0-keV transitions. The filled circles indicate the new γ rays of ^{173}W observed in the present work. The open circles indicate the γ transitions in bands 1 and 2, in which there exist transitions with energies very close to the 148.0-keV gate.

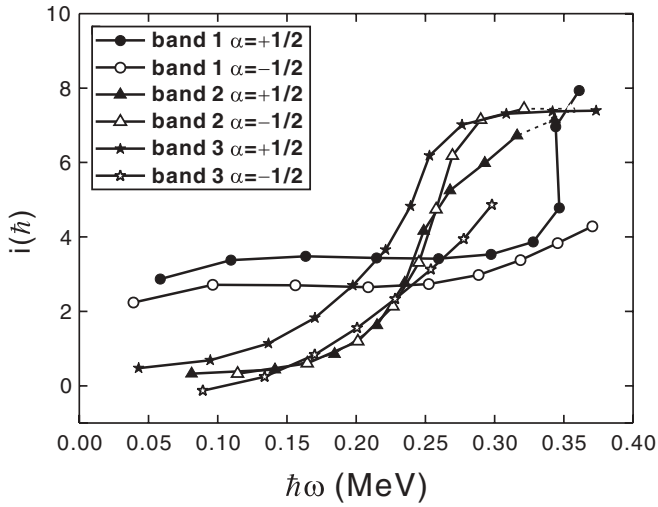

FIG. 6. Extracted alignments for bands in ^{173}W. The Harris reference parameters are chosen to be $J_0 = 34.0\hbar^2\,\mathrm{MeV}^{-1}$ and $J_1 = 75.0\hbar^4\,\mathrm{MeV}^{-3}$ for all the bands.

momentum along the rotational axis [18]. We have chosen a reference given by the Harris parameters $J_0 = 34.0\hbar^2\mathrm{MeV}^{-1}$ and $J_1 = 75.0\hbar^4\mathrm{MeV}^{-3}$ [18], which gives a nearly constant alignment in band 1 before the band crossing. One can see from Fig. 6 that the alignment curves for the rotational bands have apparent different slopes, and the upbending frequencies associated with the band crossings are also different.

A. Band 1

Band 1 is associated with the $7/2^+[633]$ configuration [4]. The two signature branches show a rather large initial alignment of approximate $3.0\hbar$, as expected for a quasineutron occupying the $7/2^+[633]$ orbit. The favored signature branch experiences a pronounced upbending at $\hbar\omega \approx 0.34$ MeV, and the band crossing could be interpreted as the neutron BC alignment [3,5]. The AD alignment in the unfavored branch was not observed in the present work. This positive-parity band displays large signature splitting in the whole spin region observed experimentally. Shastry *et al.* have systematically studied the signature splitting in the $i_{13/2}$ bands in rare-earth nuclei and pointed out that the large signature splitting is caused by the admixture of the $K = 1/2$ orbit into the odd neutron's wave functions [19].

B. Band 2

Band 2 is built on the $5/2^-[512]$ configuration [4]. One can see from Fig. 6 that the alignments of the two signature branches behave similarly. With addition of the new transitions, the band crossings are observed at $\hbar\omega \approx 0.26$ MeV for the first time. The total alignment gain is about $7.0\hbar$, consistent with the $i_{13/2}$ neutron alignment [3,5]. One interesting feature is that the alignment curves of the two signature branches cross at $\hbar\omega = 0.26$ MeV, as shown in Fig. 6.

TABLE I. Theoretical total internal conversion coefficients for some transitions in ^{173}W [15].

E_γ(keV)	Band	$\alpha_T^{th}(E1)$	$\alpha_T^{th}(E2)$	$\alpha_T^{th}(M1)$	$\alpha_T^{th}(M2)$
42.4	1			9.751	
72.1	1			12.7	
73.8	1			11.8	
114.8	1		2.31		
112.7	1			3.47	
440.5	1		0.03		
89.8	3		6.12		
148.0	$3 \rightarrow 2$	0.137	0.893	1.60	10.39
190.9	3		0.365		

Figure 7(b) presents the plot of signature splitting for this band, defined as [20]

$$S(I) = E(I) - E(I-1) - [E(I+1) - E(I) + E(I-1) - E(I-2)]/2. \quad (3)$$

Here $E(I)$ is the level energy of state I; and $S(I)$ is directly proportional to the signature splitting Δe but magnified by approximately a factor of 2. The $5/2^-[512]$ orbit is originated from the $f_{7/2}$ subshell, and therefore the branch with $\alpha = -1/2$ should be energetically favored over that with $\alpha = +1/2$. Inspecting Fig. 7(b), we can find that the $\alpha_{uf} = +1/2$ signature branch (open symbols) lies lower in energy than the $\alpha = -1/2$ one (filled symbols) at low spins; and with increasing angular momentum the two signature branches cross each other at $I = \frac{33}{2}\hbar$ and then the $\alpha = -1/2$ signature branch becomes lower in energy. This anomalous signature splitting has been referred to as low-spin signature inversion [9]. Similar phenomena were also observed in the $5/2^-[512]$ bands in the ^{171}Hf [3] and ^{175}Os [5] isotones, which are also presented in. 7 for comparison. In this chain of isotones, the inversion point shifts to lower spin with increasing proton number; the crossing spin decreases two units once, increasing by two protons.

For the prolately deformed ^{173}W isotone, the $5/2^-[512](f_{7/2})$ and $5/2^-[523](h_{9/2})$ orbits lie close to the Fermi surface; thus, the mixing between them would be expected in band 2. Qi *et al.* applied a triaxial particle rotor model (PRM) to study the signature splitting in the $5/2^-[512]$ band in ^{173}W [21]. They calculated the energy spectra $E(I)$ and signature splittings $S(I)$ assuming the valence neutron occupying the $5/2^-[512]$ and $5/2^-[523]$ orbits. The $5/2^-[512]$ and $5/2^-[523]$ orbits originate from the $f_{7/2}$ and $h_{9/2}$ subshells, respectively. Therefore, the favored signature quantum number for the $5/2^-[512]$ and $5/2^-[523]$ orbits has the opposite value. At low spins, the experimentally observed phase of $S(I)$ is consistent with that associated with the $h_{9/2}$ subshell, while at higher spins the phase of signature splitting is in agreement with that for the $f_{7/2}$ subshell. By properly mixing the $5/2^-[512]$ and $5/2^-[523]$ configurations, the observed signature inversion can be well reproduced. Therefore, they proposed that the signature inversion in band 2 is caused by the strong competition between the $5/2^-[512]$ and $5/2^-[523]$ configurations with increasing spin [21].

TABLE II. γ-ray energies, spin-parity assignments, relative γ-ray intensities, branching ratios, extracted $B(M1)/B(E2)$ values, and the $R_{ADO}(\gamma)$ values in ^{173}W.

E_γ (keV)	$J_i^\pi \rightarrow J_f^\pi$ [a]	I_γ	λ [b]	$B(M1)/B(E2)$ [c]	R_{ADO}
Decay out	transitions of	band 1			
85.3(5)	$\frac{7}{2}^+ \rightarrow \frac{5}{2}^-$	$\geqslant$897			1.02(5)
Band 1					
145.9(5)	$\frac{13}{2}^+ \rightarrow \frac{9}{2}^+$	166(13)			1.27(15)
244.0(6)	$\frac{17}{2}^+ \rightarrow \frac{13}{2}^+$	861(163)			1.36(4)
349.3(5)	$\frac{21}{2}^+ \rightarrow \frac{17}{2}^+$	1460(127)			1.29(4)
449.0(6)	$\frac{25}{2}^+ \rightarrow \frac{21}{2}^+$	1327(91)			1.33(3)
536.3(6)	$\frac{29}{2}^+ \rightarrow \frac{25}{2}^+$	1000(30)			1.25(5)
609.5(7)	$\frac{33}{2}^+ \rightarrow \frac{29}{2}^+$	797(35)			1.25(5)
668.5(6)	$\frac{37}{2}^+ \rightarrow \frac{33}{2}^+$	426(55)			1.28(7)
704.3(7)	$\frac{41}{2}^+ \rightarrow \frac{37}{2}^+$	229(61)			1.24(11)
697.2(6)	$(\frac{45}{2}^+) \rightarrow \frac{41}{2}^+$	118(12)			1.01(14)
730.0(8)	$(\frac{49}{2}^+) \rightarrow (\frac{45}{2}^+)$	67(9)			
150.0(4)	$\frac{15}{2}^+ \rightarrow \frac{13}{2}^+$	507(23)			0.72(4)
93.9(6)	$\frac{17}{2}^+ \rightarrow \frac{15}{2}^+$	147(25)			0.72(12)
245.3(5)	$\frac{19}{2}^+ \rightarrow \frac{17}{2}^+$	387(56)			0.56(5)
104.1(5)	$\frac{21}{2}^+ \rightarrow \frac{19}{2}^+$	62(15)			
336.2(5)	$\frac{23}{2}^+ \rightarrow \frac{21}{2}^+$	165(30)			0.68(6)
411.8(5)	$\frac{27}{2}^+ \rightarrow \frac{25}{2}^+$	98(16)			0.65(6)
468.8(6)	$\frac{31}{2}^+ \rightarrow \frac{29}{2}^+$	60(8)			
510.5(8)	$\frac{35}{2}^+ \rightarrow \frac{33}{2}^+$				
223.8(5)	$\frac{15}{2}^+ \rightarrow \frac{11}{2}^+$	596(46)			1.32(7)
339.1(5)	$\frac{19}{2}^+ \rightarrow \frac{15}{2}^+$	788(69)			1.35(8)
440.5(6)	$\frac{23}{2}^+ \rightarrow \frac{19}{2}^+$	693(63)			1.32(7)
524.2(6)	$\frac{27}{2}^+ \rightarrow \frac{23}{2}^+$	565(60)			1.31(6)
593.4(6)	$\frac{31}{2}^+ \rightarrow \frac{27}{2}^+$	344(84)			1.23(8)
651.5(8)	$\frac{35}{2}^+ \rightarrow \frac{31}{2}^+$	297(24)			1.26(10)
703.2(6)	$\frac{39}{2}^+ \rightarrow \frac{35}{2}^+$	199(71)			1.28(13)
751.8(8)	$(\frac{43}{2}^+) \rightarrow \frac{39}{2}^+$	87(34)			
Band 2					
266.8(6)	$\frac{11}{2}^- \rightarrow \frac{7}{2}^-$	257(30)	1.34(9)	0.23(2)	1.25(11)
353.4(6)	$\frac{15}{2}^- \rightarrow \frac{11}{2}^-$	420(38)	2.26(11)	0.26(2)	1.36(8)
419.1(6)	$\frac{19}{2}^- \rightarrow \frac{15}{2}^-$	565(143)	4.93(334)	0.18(12)	1.42(9)
465.7(6)	$\frac{23}{2}^- \rightarrow \frac{19}{2}^-$	493(88)	6.10(54)	0.19(2)	1.27(9)
499.3(6)	$\frac{27}{2}^- \rightarrow \frac{23}{2}^-$	452(81)			1.22(9)
523.8(8)	$\frac{31}{2}^- \rightarrow \frac{27}{2}^-$	409(75)			1.20(9)
544.5(6)	$\frac{35}{2}^- \rightarrow \frac{31}{2}^-$	223(47)			1.27(13)
585.2(7)	$(\frac{39}{2}^-) \rightarrow \frac{35}{2}^-$	142(32)			1.15(14)
646.5(9)	$(\frac{43}{2}^-) \rightarrow (\frac{39}{2}^-)$	99(22)			1.45(23)
714.0(9)	$(\frac{47}{2}^-) \rightarrow (\frac{43}{2}^-)$				
95.2(5)	$\frac{7}{2}^- \rightarrow \frac{5}{2}^-$	$\geqslant$217			0.66(9)
121.5(5)	$\frac{9}{2}^- \rightarrow \frac{7}{2}^-$	225(23)			0.74(6)
145.3(4)	$\frac{11}{2}^- \rightarrow \frac{9}{2}^-$	212(21)			0.65(5)
167.0(5)	$\frac{13}{2}^- \rightarrow \frac{11}{2}^-$	175(14)			0.76(4)

TABLE II. *(Continued.)*

E_γ (keV)	$J_i^\pi \rightarrow J_f^\pi$ [a]	I_γ	λ [b]	$B(M1)/B(E2)$ [c]	R_{ADO}
186.3(6)	$\frac{15}{2}^- \rightarrow \frac{13}{2}^-$	167(29)			0.84(6)
202.3(7)	$\frac{17}{2}^- \rightarrow \frac{15}{2}^-$	140(33)			0.63(5)
216.8(3)	$\frac{19}{2}^- \rightarrow \frac{17}{2}^-$	104(17)			0.86(9)
227.6(6)	$\frac{21}{2}^- \rightarrow \frac{19}{2}^-$	101(14)			0.67(8)
238.0(5)	$\frac{23}{2}^- \rightarrow \frac{21}{2}^-$	55(27)			0.61(6)
243.2(7)	$\frac{25}{2}^- \rightarrow \frac{23}{2}^-$				
256.0(5)	$\frac{27}{2}^- \rightarrow \frac{25}{2}^-$				
216.6(5)	$\frac{9}{2}^- \rightarrow \frac{5}{2}^-$	95(15)	0.53(4)	0.35(4)	1.21(17)
312.3(5)	$\frac{13}{2}^- \rightarrow \frac{9}{2}^-$	299(17)	1.80(9)	0.25(2)	1.37(9)
388.8(6)	$\frac{17}{2}^- \rightarrow \frac{13}{2}^-$	483(70)	3.64(19)	0.21(1)	1.22(6)
444.3(5)	$\frac{21}{2}^- \rightarrow \frac{17}{2}^-$	509(70)	5.14(27)	0.20(1)	1.34(8)
481.0(7)	$\frac{25}{2}^- \rightarrow \frac{21}{2}^-$	504(72)			1.36(8)
505.8(7)	$\frac{29}{2}^- \rightarrow \frac{25}{2}^-$	434(58)			1.32(8)
542.5(8)	$\frac{33}{2}^- \rightarrow \frac{29}{2}^-$	291(45)			1.29(11)
591.6(5)	$\frac{37}{2}^- \rightarrow \frac{33}{2}^-$	221(32)			1.23(10)
637.4(8)	$(\frac{41}{2}^-) \rightarrow \frac{37}{2}^-$	144(31)			1.32(13)
691.0(10)	$(\frac{45}{2}^-) \rightarrow (\frac{41}{2}^-)$				
Decay out	transitions of	band 3			
148.0(5)	$\frac{1}{2}^- \rightarrow \frac{5}{2}^-$	$\geqslant$74			
Band 3					
89.8(5)	$\frac{5}{2}^- \rightarrow \frac{1}{2}^-$	$\geqslant$28			
190.9(5)	$\frac{9}{2}^- \rightarrow \frac{5}{2}^-$	564(53)			1.50(5)
274.5(5)	$\frac{13}{2}^- \rightarrow \frac{9}{2}^-$	521(30)			1.26(4)
341.2(6)	$\frac{17}{2}^- \rightarrow \frac{13}{2}^-$	552(56)			1.30(3)
395.7(7)	$\frac{21}{2}^- \rightarrow \frac{17}{2}^-$	497(39)			1.25(3)
442.4(6)	$\frac{25}{2}^- \rightarrow \frac{21}{2}^-$	490(48)			1.24(4)
479.0(6)	$\frac{29}{2}^- \rightarrow \frac{25}{2}^-$	372(30)			1.30(5)
506.8(6)	$\frac{33}{2}^- \rightarrow \frac{29}{2}^-$	344(31)			1.20(5)
552.8(7)	$\frac{37}{2}^- \rightarrow \frac{33}{2}^-$	215(19)			1.30(7)
616.8(8)	$\frac{41}{2}^- \rightarrow \frac{37}{2}^-$	137(11)			1.21(9)
683.8(8)	$(\frac{45}{2}^-) \rightarrow \frac{41}{2}^-$	64(13)			
747.0(9)	$(\frac{49}{2}^-) \rightarrow (\frac{45}{2}^-)$	44(6)			
181.5(4)	$\frac{7}{2}^- \rightarrow \frac{3}{2}^-$	189(29)			1.31(8)
269.1(5)	$\frac{11}{2}^- \rightarrow \frac{7}{2}^-$	60(5)			1.29(9)
341.0(6)	$\frac{15}{2}^- \rightarrow \frac{11}{2}^-$	67(22)			1.49(10)
402.1(5)	$\frac{19}{2}^- \rightarrow \frac{15}{2}^-$	51(6)			1.25(10)
457.0(5)	$\frac{23}{2}^- \rightarrow \frac{19}{2}^-$	46(7)			1.33(9)
508.3(8)	$(\frac{27}{2}^-) \rightarrow \frac{23}{2}^-$	49(8)			
555.8(5)	$(\frac{31}{2}^-) \rightarrow (\frac{27}{2}^-)$	31(6)			
596.6(4)	$(\frac{35}{2}^-) \rightarrow (\frac{31}{2}^-)$				

[a] See text for details about the spin and parity assignments.

[b] Branching ratio: $T_\gamma(I \rightarrow I-2)/T_\gamma(I \rightarrow I-1)$. Here $T_\gamma(I \rightarrow I-2)$ and $T_\gamma(I \rightarrow I-1)$ are the γ-ray intensities of the $\Delta I = 2$ and $\Delta I = 1$ transitions, respectively. These intensities were measured in a summed coincidence spectrum gated by the transitions above the state of interest.

[c] See Eq. (2). Here, the $B(M1)/B(E2)$ values are extracted from the branching ratios λ by assuming $\delta^2 = 0$.

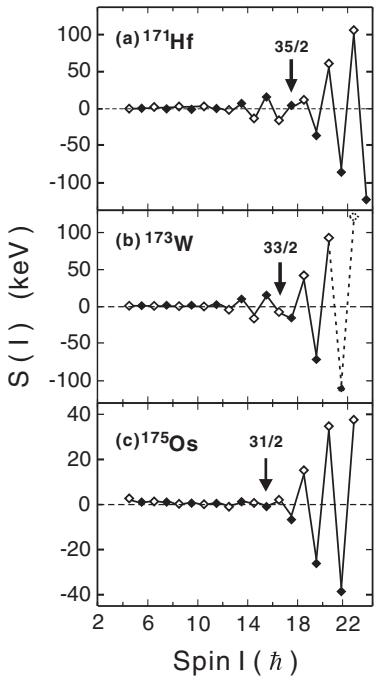

FIG. 7. Systematics of the signature splittings of the $5/2^-[512]$ bands in ^{171}Hf [3], ^{173}W (this work), and ^{175}Os [5]. The opened (filled) symbols correspond to the $\alpha = +1/2$ ($\alpha = -1/2$) signature. The arrows indicate the signature-crossing spins.

As is well known, the in-band decay properties can provide a sensitive test for configuration assignments. Information on the specific intrinsic orbit of band 2 can be obtained by comparing theoretical $B(M1)/B(E2)$ values with experimental ones. The experimental $B(M1)/B(E2)$ values were deduced according to Eq. (2) described previously. The theoretical ratios are estimated using the semiclassical formula [22,23]

$$\frac{B(M1; I \to I-1)}{B(E2; I \to I-2)} = \frac{12}{5Q_0^2 \cos^2(\gamma + 30^\circ)} \left[1 - \frac{K^2}{(I-1/2)^2}\right]^{-2} \frac{K^2}{I^2} \times \{(g_1 - g_R)[(I^2 - K^2)^{1/2} - i_1]\}^2 \left(\frac{\mu_N^2}{e^2\,\mathrm{b}^2}\right). \quad (4)$$

This expression takes into account the effect of triaxiality γ on the $E2$ transition rate. In the calculations, the intrinsic quadrupole moment Q_0 was set to be 6.0 e b, a characteristic value in this region. The gyromagnetic factor g_1 was adopted from the values in ^{171}Hf [3] and ^{175}Os [5]. The rotational gyromagnetic factor $g_R = 0.3$ was taken from Refs. [24,25]. The aligned angular momentum of the strongly coupled particle was set to be $i_1 = 0.6\hbar$ as deduced from experiment (see Fig. 6). The nominal bandhead K was 2.5. We used $\gamma = 0^\circ$ in the calculations. The calculated results under the assumption of the $5/2^-[512]$ and $5/2^-[523]$ configurations are presented in the middle panel of Fig. 8 in comparison with the experimental data. It is clear that the experimental $B(M1)/B(E2)$ ratios are very close to the theoretical values of the $5/2^-[512]$ orbit in the whole spin region covered

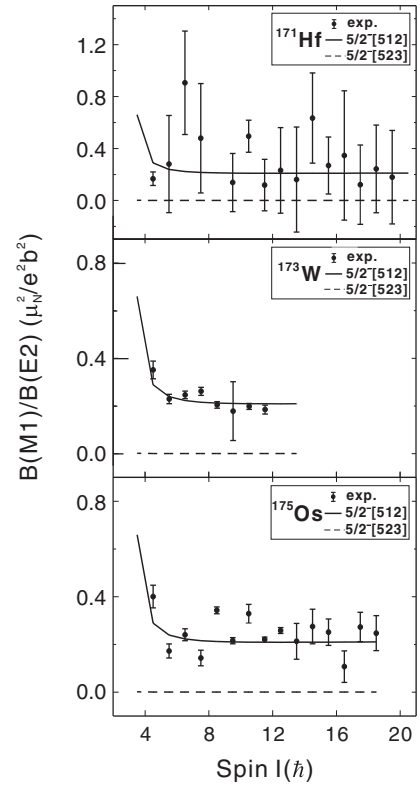

FIG. 8. Comparison of the experimental and theoretical $B(M1)/B(E2)$ values for the $5/2^-[512]$ bands in ^{171}Hf [3], ^{173}W (this work), and ^{175}Os [5]. The theoretical values are calculated under the assumptions of the $5/2^-[512]$ and $5/2^-[523]$ orbits, respectively.

experimentally, but they are far away from the expected values of the $5/2^-[523]$ orbit. Therefore, we might conclude that the $5/2^-[512]$ orbit originating from the $f_{7/2}$ subshell is always overwhelmingly dominant in the configurations of the states. It should be noted that the $5/2^-[512]$ band in ^{175}Os was suggested to be mainly associated with the $5/2^-[512]$ configuration without appreciable admixture of the $5/2^-[523]$ orbit by the analysis of experimentally measured g factors [5]. The experimental and theoretical $B(M1)/B(E2)$ ratios of the $5/2^-[512]$ bands in ^{171}Hf and ^{175}Os are also plotted in Fig. 8 for comparison. The transition energies and intensities used to deduce the experimental values were taken from Refs. [3,5] and it is noted that the λ values used to deduce the $B(M1)/B(E2)$ ratios of ^{171}Hf and ^{175}Os are calculated from the individual γ-ray intensities in Table I of Ref. [3] and Table 3 of Ref. [3]. The theoretical calculations are the same as those for ^{173}W. Examining Fig. 8, one can see that the experimental data in the $N = 99$ isotones show almost identical behaviors up to the highest states observed, and these can be well reproduced by assuming the $5/2^-[512]$ configuration. In other words, the $5/2^-[512]$ bands in the isotones have a quite pure $5/2^-[512]$ configuration, and the admixture of the $5/2^-[523]$ configuration is small. Therefore, the signature inversions in the $5/2^-[512]$ bands could not be explained by the mechanism of configuration mixing [21]. Further theoretical efforts are needed to study the band properties associated with the $5/2^-[512]$ configuration.

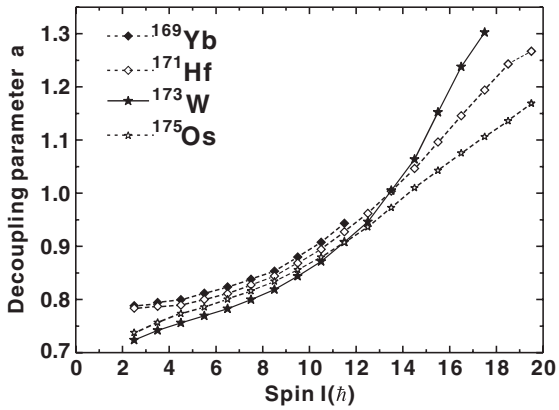

FIG. 9. Decoupling parameters as a function of spin for the $1/2^-[521]$ bands in the $N = 99$ isotones. In the calculation, the relative energy between the $3/2^-$ and $1/2^-$ states of band 3 in ^{173}W is assumed to be 71 keV.

C. Band 3

Band 3 is based on the $1/2^-[521]$ orbit [4]. Comparing the level spacings of band 3 with those of the $1/2^-[521]$ bands in the neighboring isotones (^{169}Yb [13], ^{171}Hf [3], and ^{175}Os [5]) and heavier odd-A W isotopes [4,13,14], we can find that band 3 in ^{173}W follows the trends very well. According to the systematics of the energy differences between the $1/2^-$ and $3/2^-$ states, we assume that the $3/2^-$ state is located 71 keV above the $1/2^-$ state in ^{173}W, and this energy is used in the following analysis. The level energies in a decoupled band can be described by the formula

$$E(I) = \frac{\hbar^2}{2\Im}[I(I+1) + a(-1)^{I+1/2}(I+1/2)]. \qquad (5)$$

The decoupling parameter a is very characteristic for the configuration involved. We deduced the decoupling parameter of band 3 from the excitation energies of the levels concerned. It turns out that a falls in the range $0.75 < a < 0.85$ at low spins, and the experimental value is in agreement with the $1/2^-[521]$ configuration assignment [5]. Figure 9 shows the decoupling parameters for the $1/2^-[521]$ bands in the $N = 99$ isotones (^{169}Yb [13], ^{171}Hf [3], and ^{175}Os [5]). It can be seen that the decoupling parameters in the isotones behave similarly, and they increase gradually with increasing spins. Since the decoupling parameter $a \approx i_x(\omega, \alpha = +1/2) - i_x(\omega, \alpha = -1/2)$ [5], the observed increasing parameter indicates that the alignment of the favored signature branch might increase more quickly than that of the unfavored branch. As shown in Fig. 6, the favored signature branch of the $1/2^-[521]$ band in ^{173}W undergoes an AB neutron crossing at $\hbar\omega \approx 0.24$ MeV with an alignment gain of about $7.0\hbar$. For the unfavored branch, the AB neutron crossing is delayed by at least 30 keV with respect to that of the favored branch and a complete band crossing is not in sight at the last transition observed. Similar shifts were observed in the $1/2^-[521]$ bands in the isotones ^{171}Hf [3] and ^{175}Os [5]. This might be an indication of different shape-driving effects of the two signatures associated with the $1/2^-[521]$ orbits in the $N = 99$ isotones [5].

V. SUMMARY

The odd-A nucleus ^{173}W has been produced in the bombardment of a ^{150}Nd target with ^{28}Si projectiles. The previously known $7/2^+[633]i_{13/2}$, $5/2^-[512]$, and $1/2^-[521]$ bands have been extended up to $(49/2\hbar)$, $(47/2\hbar)$, and $(49/2\hbar)$ states, respectively. A newly identified sequence has been suggested to be the unfavored signature branch of the $1/2^-[521]$ band by comparing the level spacings and decoupling parameters with those of the $1/2^-[521]$ bands in the heavier W isotopes. The band crossing of the $5/2^-[512]$ band is observed for the first time, and it is attributed to the $i_{13/2}$ neutron alignment. The $5/2^-[512]$ band shows low-spin signature inversion, and the normal signature splitting is restored after the band crossing. The signature splittings of the $5/2^-[512]$ bands in the $N = 99$ isotones are very similar, and the spin values of the signature-inversion points show a regular pattern. By comparing the measured $B(M1)/B(E2)$ ratios with the theoretical values, we conclude that the configuration of the $5/2^-[512]$ bands in the isotones is quite pure without appreciable admixture of the $5/2^-[523]$ orbit. This is inconsistent with the PRM calculated results, which explains the signature inversion by the strong competition between the $5/2^-[512]$ and $5/2^-[523]$ orbits. The mechanism of the low-spin signature inversion in the $5/2^-[512]$ bands is still an open question and deserves to be further studied theoretically.

ACKNOWLEDGMENTS

The authors wish to thank the staff of the JAEA tandem accelerator for providing the ^{28}Si beam and their hospitality during the experiment. This work was supported by the National Natural Sciences Foundation of China (Grants No. 11175217, No. 10825522, and No. GJ073005), the Major State Basic Research Development Program of China (Grant No. 2007CB815000), and the Chinese Academy of Sciences.

[1] L. Chen *et al.*, Phys. Rev. C **83**, 034318 (2011), and references therein.
[2] S. T. Wang *et al.*, Phys. Rev. C **84**, 017303 (2011), and references therein.
[3] D. M. Cullen *et al.*, Nucl. Phys. A **673**, 3 (2000).
[4] P. M. Walker, G. D. Dracoulis, A. Johnston, J. R. Leigh, M. G. Slocombe, and I. F. Wright, J. Phys. G **4**, 1655 (1978).
[5] B. Fabricius, G. D. Dracoulis, R. A. Bark, A. E. Stuchbery, T. Kibèdi, and A. M. Baxter, Nucl. Phys. A **511**, 345 (1990).
[6] G. S. Li *et al.*, J. Phys. G **38**, 095105 (2011), and references therein.
[7] X. H. Zhou *et al.*, Phys. Rev. C **75**, 034314 (2007), and references therein.
[8] I. Hamamoto, Nucl. Phys. A **520**, c297 (1990).
[9] R. Bengtsson, H. Frisk, F. R. May, and J. A. Pinston, Nucl. Phys. A **415**, 189 (1984).
[10] D. J. Hartley *et al.*, Phys. Rev. C **58**, 2720 (1998).
[11] O. Zeidan *et al.*, Phys. Rev. C **65**, 024303 (2002).

[12] M. Oshima, Y. Toh, Y. Hatsukawa, M. Koizumi, A. Kimura, A. Haraga, M. Ebihara, and K. Sushida, J. Radioanal. Nucl. Chem. **278**, 257 (2008).
[13] http://www.nndc.bnl.gov/ensdf/.
[14] F. M. Bernthal and R. A. Warner, Phys. Rev C **11**, 188 (1975).
[15] http://www.nndc.bnl.gov/hsicc/.
[16] F. G. Kondev, Nucl. Data Sheets **98**, 1073 (2003).
[17] S. Juutinen *et al*., Nucl. Phys. A **526**, 346 (1991).
[18] R. Bengtsson and S. Frauendorf, Nucl. Phys. A **327**, 139 (1979).
[19] S. Shastry, J. C. Bacelar, J. D. Garrett, G. B. Hagemann, B. Herskind, and J. Kownacki, Nucl. Phys. A **470**, 253 (1987).
[20] Y. H. Zhang, T. Hayakawa, M. Oshima, J. Katakura, Y. Hatsukawa, M. Matsuda, H. Kusakari, M. Sugawara, T. Komatsubara, and K. Furuno, Phys. Rev. C **65**, 014302 (2001).
[21] B. Qi, S. Q. Zhang, S. Y. Wang, and J. Meng, Int. J. Mod. Phys. E **18**, 109 (2009).
[22] A. J. Larabee, L. H. Courtney, S. Frauendorf, L. L. Riedinger, J. C. Waddington, M. P. Fewell, N. R. Johnson, I. Y. Lee, and F. K. McGowan, Phys. Rev. C **29**, 1934 (1984).
[23] F. Dönau, Nucl. Phys. A **471**, 469 (1987).
[24] S. K. Tandel *et al*., Phys. Rev. C **73**, 044306 (2006).
[25] M. Ionescu-Bujor *et al*., Phys. Lett. B **495**, 289 (2000).